Available online at www.sciencedirect.com
ScienceDirect
Trans. Nonferrous Met. Soc. China 26(2016) 406−413
Transactions of Nonferrous Metals Society of China
www.tnmsc.cn

Wear behavior of Mg−10Y−4Gd−1.5Zn−0.4Zr alloy

Mao-liang HU[1], Qu-dong WANG[2], Ze-sheng JI[1], Hong-yu XU[1], Ming-de XIN[1], Guo-rui MA[3]

1. School of Materials Science and Engineering, Harbin University of Science and Technology, Harbin 150040, China;
2. National Engineering Research Center for Light Alloy Net Forming, Shanghai Jiao Tong University, Shanghai 200240, China;
3. College of Materials Science and Chemical Engineering, Harbin Engineering University, Harbin 150001, China

Received 27 February 2015; accepted 21 July 2015

Abstract: Dry sliding wear tests were performed on a Mg−10Y−4Gd−1.5Zn−0.4Zr alloy using a Ball-on-Flat type wear apparatus against an AISI 52100 type bearing steel ball counterface. The wear rates were measured within a load range of 3−25 N, a sliding speed range of 0.03−0.3 m/s and a sliding temperature range of 25−200 °C at a constant sliding distance of 400 m. The morphologies of the worn surfaces and wear debris were studied by scanning electron microscopy (SEM) and energy dispersive X-ray spectroscopy (EDS). Comparatively, the wear properties of a hypereutectic Al−Si aluminium alloy under the same condition were measured. The results indicate that the wear rates of Mg−10Y−4Gd−1.5Zn−0.4Zr alloy are lower than that of cast+T6 AC9B aluminium alloy. The dominant mechanism of cast+T6 Mg−10Y−4Gd−1.5Zn−0.4Zr alloy is abrasion wear mixed with other wear mechanisms, which tends to be an abrasion and plastic deformation wear at high normal load such as 10−25 N, abrasion and plastic deformation wears with small participation of delamination and oxidative wears at high sliding speed such as 0.12−0.3 m/s, and an oxidative and abrasion wear at high test temperature such as 100−200 °C. The $Mg_{12}Y_1Zn_1$ phase in Mg−10Y−4Gd−1.5Zn−0.4Zr alloy plays an important role in the wear rate.

Key words: Mg−Y−Gd−Zn−Zr alloy; sliding wear; wear rate; wear mechanism; hypereutectic Al−Si alloy

1 Introduction

Magnesium and its alloys are of considerable interest to automobile and aerospace industries because of their low densities, excellent castability and high specific strength [1]. In recent years, new magnesium alloys have been proposed incorporating rare earth elements to improve their characteristics for wider applications [2,3]. Rare earth can purify the alloy melt, refine the microstructure and improve the mechanical properties of magnesium alloys. However, the use of magnesium alloys is limited because of their poor surface properties such as wear resistance [4]. The poor wear resistance prevents these magnesium alloys from being used as widely as aluminium alloys. It is considerable interest in valuating the wear properties of magnesium alloys.

There are some researches dealing with the wear properties of conventional magnesium alloys such as AZ31 [5,6], AZ61 [7,8] and AZ91 [9,10]. In these researches, the wear mechanisms including abrasion, oxidation, delamination, adhesion, thermal softening and melting were proposed. The friction coefficient of AZ31B magnesium alloy is extremely low compared with that of 5083 aluminium alloy for the non-lubed sheet metals [11]. The affinity between AZ31B magnesium alloy and tool steel is very low compared with that between 5083 aluminium alloy and tool steel. The wear rate of AZ91D magnesium alloy is lower than that of AS21 aluminium alloy against sintered iron alloy [12]. Recently, HU et al [13] have reported that the wear rate of Mg−10Gd−3Y−0.4Zr alloy is lower than that of near-eutectic Al−Si aluminium alloy. Mg−11Y−5Gd−2Zn alloy shows lower wear rate [14]. However, Zr addition has an important effect on the grain refinement of magnesium alloys. The addition of Zn improves the castability and creep resistance of magnesium alloys.

Foundation item: Project (51404082) supported by the National Natural Science Foundation of China; Project (E201442) supported by the Natural Science Foundation of Heilongjiang Province, China; Project (12531116) supported by the Foundation of Educational Committee of Heilongjiang Province, China; Project (2013RFQXJ137) supported by the Harbin Special Funds for Creative Talents in Science and Technology, China; Project (201510) supported by Science Funds for the Young Innovative Talents of HUST, China

Corresponding author: Mao-liang HU; Tel: +86-451-86392501; E-mail: humaoliang@hrbust.edu.cn

DOI: 10.1016/S1003-6326(16)64092-X

Few studies have been carried out to understand the sliding wear properties of Mg−Y−Gd−Zn−Zr alloys. There is a lack of studies for wear properties between magnesium alloy and hypereutectic Al−Si aluminium alloy under the same condition.

The purpose of this work is to better understand the wear properties of Mg−10Y−4Gd−1.5Zn−0.4Zr alloy. The role of the normal load, sliding speed and sliding temperature on the wear properties was studied. The present work was also designed to study the difference of wear properties between Mg−Y−Gd−Zn−Zr alloy and hypereutectic Al−Si aluminium alloy under the same condition.

2 Experimental

Mg−Y−Gd−Zn−Zr alloy was prepared from high purity Mg (99.95%), Zn (99.99%) and master alloys of Mg−25%Y, Mg−25%Gd and Mg−30%Zr (mass fraction) in an electric resistance furnace under a mixed protective gas of CO_2 and SF_6 with a volume ratio of 100:1. Then, a steel mould was pre-heated to 150 °C and the alloy was cast into the steel mould. Table 1 shows the actual composition of the cast ingot measured using inductively coupled plasma-atomic emission spectroscopy (ICP-AES). Rectangular samples were cut from the ingot using electric spark linear cutting. These samples were solution heat-treated at 525 °C for 20 h and then aged at 225 °C for 24 h in a hot oil bath followed by quenching in cold water. Table 2 shows the physical and mechanical properties of Mg−10Y−4Gd−1.5Zn−0.4Zr alloy and AC9B aluminium alloys at 25 °C.

Table 1 Chemical composition of Mg−10Y−4Gd−1.5Zn−0.4Zr alloy (mass fraction, %)

Y	Gd	Zn	Zr	Mg
9.8	4.21	1.66	0.38	Bal.

AC9B aluminium alloy is a hypereutectic Al−Si alloy and its chemical composition is 18.4% Si, 0.83% Mg, 1.35% Cu, 1.39% Ni and balance Al. AC9B aluminium alloy was solution heat-treated at 520 °C for 4 h and then aged at 175 °C for 8 h in a hot oil bath followed by quenching in cold water. AC9B aluminium alloys are widely used in the automotive industry in piston applications [15,16].

The wear tests were carried out under dry sliding condition in accordance with the ASTM G133−02 standard [17] using a Ball-on-Flat wear testing machine. The rectangular samples (50 mm × 30 mm × 5 mm) of Mg and Al alloys were ground manually by 240, 800, 1500 and 2400 grit SiC papers. The counterface was a ball with 6 mm in diameter made of AISI 52100 type bearing steel [13].

The tests were carried out in a normal load range of 3−25 N, a sliding speed range of 0.03−0.3 m/s and a sliding temperature range of 25−200 °C at a constant sliding distance of 400 m. The mass losses were weighed before and after the sliding tests after removing any loose debris using a precision balance (0.1 mg) [13]. Each test was carried out at least twice in order to check the reproducibility and the deviation between two tests was within 4%. The average value of the tests was taken to determine the wear rate.

The worn surfaces were examined using scanning electron microscopy (SEM) equipped with energy dispersive X-ray spectroscopy (EDS) and the wear debris was collected from the worn surface. Since the hardness of steel ball was far higher than that of the sample and its wear loss was very small, the wear properties of the steel ball are not studied in the present work.

3 Results and discussion

3.1 Initial microstructure

Figure 1 shows the initial microstructures of AC9B aluminium alloy and Mg−10Y−4Gd−1.5Zn−0.4Zr alloy. AC9B aluminium alloy is a hypereutectic Al−Si alloy with coarse primary silicon particles and fine plate-like eutectic silicon particles, as shown in Fig. 1(a). These silicon particles mainly improve the wear and mechanical properties of Al−Si alloys [16,18−20]. AC9B aluminium alloy is suited to automotive industry in piston applications, referred to as piston alloy.

For Mg−10Y−4Gd−1.5Zn−0.4Zr alloy, its microstructure contains four different phases, namely: the α-Mg matrix, the eutectic compound $Mg_{24}(GdYZn)_5$,

Table 2 Physical and mechanical properties of Mg−10Y−4Gd−1.5Zn−0.4Zr alloy and AC9B aluminium alloys at 25 °C

Alloy	Density/ ($g \cdot cm^{-3}$)	Hardness (HV_5)	Elastic modulus/GPa	Ultimate tensile strength/MPa	Yield strength/MPa	Elongation to failure/%
Mg−10Y−4Gd−1.5Zn−0.4Zr alloy (as-cast)	1.99	101.5	−	178	−	0.59
Mg−10Y−4Gd−1.5Zn−0.4Zr alloy (cast+T6)	1.99	129.0	45.36	306	249	1.37
AC9B aluminium alloy (cast+T6)	2.69	131.2	85.12	276	−	1.26

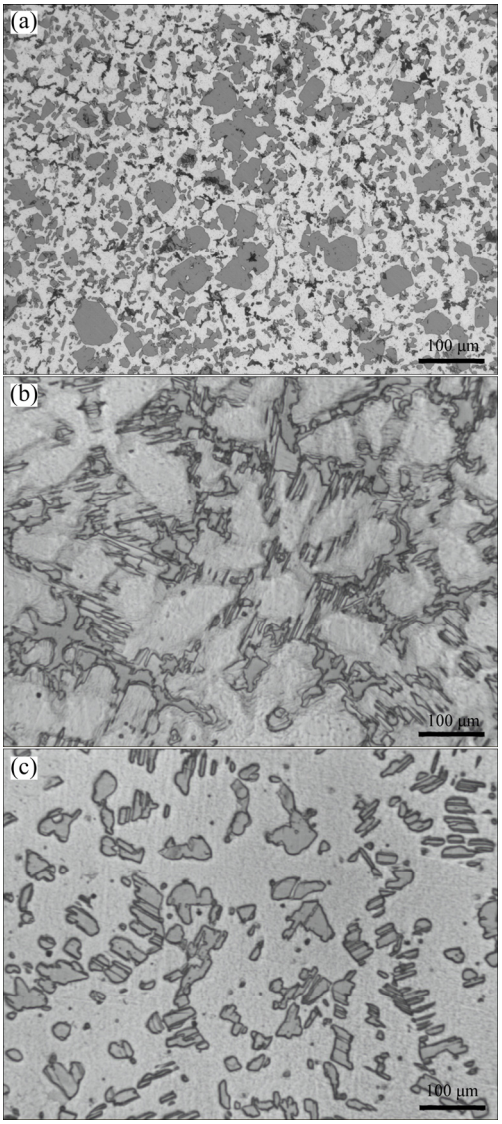

Fig. 1 Initial microstructures of plate samples: (a) Cast+T6 AC9B aluminium alloy; (b) As-cast Mg−10Y−4Gd−1.5Zn−0.4Zr alloy; (c) Cast+T6 Mg−10Y−4Gd−1.5Zn−0.4Zr alloy

the long-period stacking ordered structure phase $Mg_{12}Y_1Zn_1$ and intracrystalline Zr-rich cores, as shown in Figs. 1(b) and (c). The eutectic compound $Mg_{24}(GdYZn)_5$ is network-shaped and distributed mostly in the grain boundaries and triple points [21,22]. The $Mg_{12}Y_1Zn_1$ phase is a needle-like one and distributed from eutectic compound to α-Mg matrix. The Zr-rich core has an important effect on the grain refinement and greatly improves the mechanical properties [23]. The Zr-rich core is present in the grains or near the grain boundaries. After solution heat-treated at 525 °C for 20 h and aged at 225 °C for 24 h, the amount of $Mg_{24}(GdYZn)_5$ phase significantly decreases. At the same time, the amount of $Mg_{12}Y_1Zn_1$ phase increases. There were some researches dealing with the microstructure and mechanical properties of Mg−Y−Gd−Zn−Zr alloys [21,22,24].

3.2 Wear rate

Figure 2 shows the effect of normal load on the wear rate of as-cast Mg−10Y−4Gd−1.5Zn−0.4Zr alloy, cast+T6 Mg−10Y−4Gd−1.5Zn−0.4Zr alloy and cast+T6 AC9B aluminium alloy. The sliding speed was 0.06 m/s, the sliding temperature was 25 °C and the sliding distance was 400 m. For all the tested flat samples, the wear rate increases significantly with increasing the normal load. At low normal loads of 3, 5 and 7 N, the wear rate of cast+T6 AC9B aluminium alloy is almost the same as that of as-cast Mg−10Y−4Gd−1.5Zn−0.4Zr alloy. At high normal loads (F>7 N), the wear rate of cast+T6 AC9B aluminium alloy is two times that of cast+T6 Mg−10Y−4Gd−1.5Zn−0.4Zr alloy. The wear rate of cast+T6 Mg−10Y−4Gd−1.5Zn−0.4Zr alloy is lower than that of as-cast Mg−10Y−4Gd−1.5Zn−0.4Zr alloy. The difference in value increases rapidly with increasing the normal load at high normal loads (F>7 N).

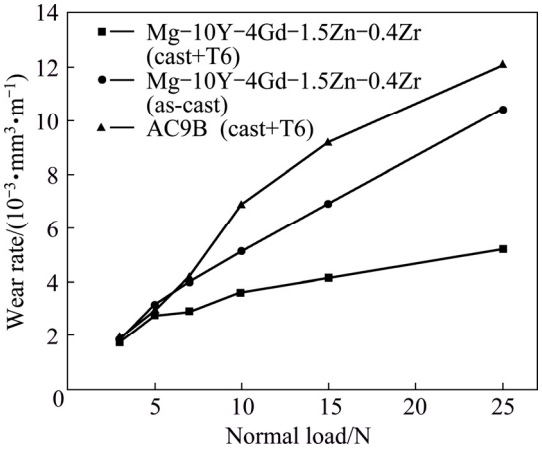

Fig. 2 Effect of normal load on wear rate of as-cast Mg−10Y−4Gd−1.5Zn−0.4Zr alloy, cast+T6 Mg−10Y−4Gd−1.5Zn−0.4Zr alloy and cast+T6 AC9B aluminium alloy (Sliding speed of 0.06 m/s, sliding temperature of 25 °C and sliding distance of 400 m)

Figure 3 shows the effect of sliding speed on the wear rate of as-cast Mg−10Y−4Gd−1.5Zn−0.4Zr alloy, cast+T6 Mg−10Y−4Gd−1.5Zn−0.4Zr alloy and cast+T6 AC9B aluminium alloy. The normal load was 10 N, the sliding temperature was 25 °C and the sliding distance was 400 m. The wear rate decreases obviously with increasing the sliding speed for all the tested flat samples. Cast+T6 AC9B aluminium alloy has higher wear rate than Mg−10Y−4Gd−1.5Zn−0.4Zr alloy. The wear rate of cast+T6 AC9B aluminium alloy is about two times that of cast+T6 Mg−10Y−4Gd−1.5Zn−0.4Zr alloy. At low sliding speeds of 0.03, 0.06 and 0.12 m/s, as-cast Mg−10Y−4Gd−1.5Zn−0.4Zr alloy has higher wear rate than cast+T6 Mg−10Y−4Gd−1.5Zn−0.4Zr alloy. At high sliding speeds of 0.18, 0.24 and 0.3 m/s, as-cast Mg−10Y−4Gd−1.5Zn−0.4Zr alloy has lower wear rate

than cast+T6 Mg−10Y−4Gd−1.5Zn−0.4Zr alloy. The decrease of wear rate of as-cast Mg−10Y−4Gd−1.5Zn−0.4Zr alloy is higher than that of cast+T6 Mg−10Y−4Gd−1.5Zn−0.4Zr alloy.

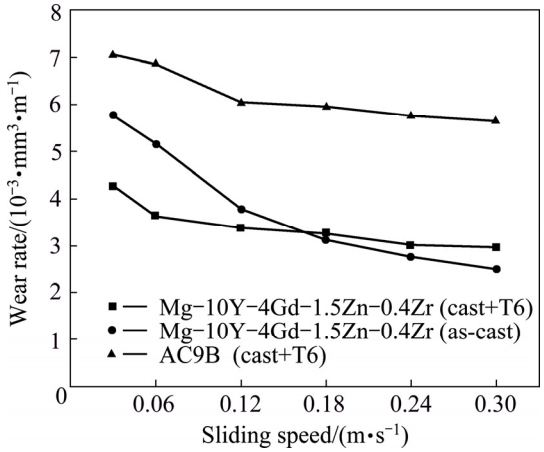

Fig. 3 Effect of sliding speed on wear rate of as-cast Mg−10Y−4Gd−1.5Zn−0.4Zr alloy, cast+T6 Mg−10Y−4Gd−1.5Zn−0.4Zr alloy and cast+T6 AC9B aluminium alloy (Normal load of 10 N, sliding temperature of 25 °C and sliding distance of 400 m)

Figure 4 shows the effect of sliding temperature on the wear rate of as-cast Mg−10Y−4Gd−1.5Zn−0.4Zr alloy, cast+T6 Mg−10Y−4Gd−1.5Zn−0.4Zr alloy and cast+T6 AC9B aluminium alloy. The normal load was 10 N, the sliding speed was 0.06 m/s and the sliding distance was 400 m. It is evident from Fig. 4 that the wear rate of cast+T6 AC9B aluminium alloy increases as the sliding temperature increases and it climbs quickly at 150 °C. Cast+T6 AC9B aluminium alloy has higher wear rate than Mg−10Y−4Gd−1.5Zn−0.4Zr alloy. For Mg−10Y−4Gd−1.5Zn−0.4Zr alloy, the wear rate exhibits the maximum value at 100 °C and descends with

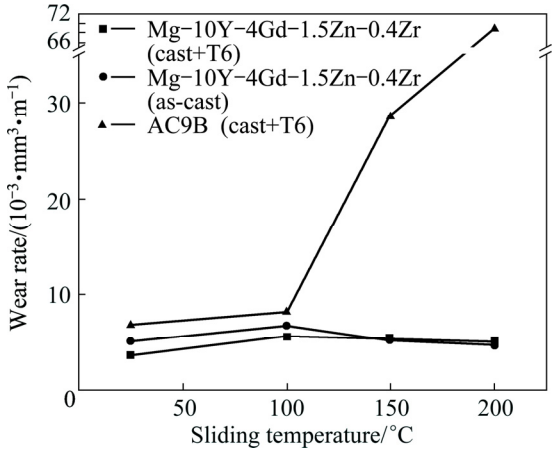

Fig. 4 Effect of sliding temperature on wear rate of as-cast Mg−10Y−4Gd−1.5Zn−0.4Zr alloy, cast+T6 Mg−10Y−4Gd−1.5Zn−0.4Zr alloy and cast+T6 AC9B aluminium alloy (Normal load of 10 N, sliding speed of 0.06 m/s and sliding distance of 400 m)

increasing the sliding temperature from 100 to 200 °C. At low sliding temperatures of 25 and 100 °C, as-cast Mg−10Y−4Gd−1.5Zn−0.4Zr alloy has higher wear rate than cast+T6 Mg−10Y−4Gd−1.5Zn−0.4Zr alloy. At high sliding temperatures of 150 and 200 °C, as-cast Mg−10Y−\4Gd−1.5Zn−0.4Zr alloy has slightly lower wear rate than cast+T6 Mg−10Y−4Gd−1.5Zn−0.4Zr alloy.

For the Mg−10Y−4Gd−1.5Zn−0.4Zr alloy, the $Mg_{24}(GdYZn)_5$ eutectic phase was homogeneously dispersed at the grain boundaries and triple points [21]. The $Mg_{24}(GdYZn)_5$ eutectic phase has a strengthening effect on the alloys at temperature lower than 250 °C and improves the wear properties. HU et al [13] suggested that the more the amount of $Mg_{24}(GdYZn)_5$ eutectic phase, the lower the wear rate of its alloy. In the present study, the amount of $Mg_{24}(GdYZn)_5$ phase of as-cast alloy is more than that of cast+T6 alloy, but the wear rate of as-cast alloy is higher than that of cast+T6 alloy. After solution heat-treated and aged, the amount of $Mg_{24}(GdYZn)_5$ phase significantly decreases. At the same time, the amount of $Mg_{12}Y_1Zn_1$ phase increases. The $Mg_{12}Y_1Zn_1$ phase also has a strengthening effect on the alloys. In the process of the solution heat-treatment and aging, the grain size does not change. The effect of grain size on the wear rate is negligibly small. Comparatively, the effect of $Mg_{12}Y_1Zn_1$ phase on wear resistance is higher than that of $Mg_{24}(GdYZn)_5$ phase. As a result, the wear rate of cast+T6 Mg−10Y−4Gd−1.5Zn−0.4Zr alloy is lower than that of as-cast alloy at room temperature. Higher sliding speed or sliding temperature results in higher contact temperature. At higher temperature, the $Mg_{12}Y_1Zn_1$ phase is associated with the softening and attributes to a decrease in resisting the material flow [14]. The effect of $Mg_{12}Y_1Zn_1$ phase on the wear resistance decreases, as shown in Figs. 3 and 4. Therefore, the wear rate of cast+T6 Mg−10Y−4Gd−1.5Zn−0.4Zr alloy is higher than that of as-cast alloy at higher sliding speed (S>0.12 m/s) or higher sliding temperature (t>100 °C).

For hypereutectic Al−Si alloys, a considerable amount of work has been reported on the wear mechanism [18−20]. AC9B aluminium alloy is suited to automotive industry in piston application. The coarse primary silicon particles and fine plate-like eutectic silicon particles of AC9B aluminium alloy play an important role in improving the wear properties. The difference of wear properties between Mg−Y−Gd−Zn−Zr alloy and hypereutectic Al−Si aluminium alloy under the same condition is present. The worn surface and wear debris of AC9B aluminium alloy are not studied. Comparatively, it is evident that the wear rate of AC9B aluminium alloys is higher than that of Mg−10Y−4Gd−1.5Zn−0.4Zr alloy under the same conditions.

3.3 Worn surface

Figure 5 shows the SEM images of worn surfaces of cast+T6 Mg−10Y−4Gd−1.5Zn−0.4Zr alloy. Table 3 shows the EDS results of testing areas in Fig. 5. At low load of 3 N, the worn surface is covered with numerous shallow grooves, as shown in Fig. 5(a). These grooves are parallel to the sliding direction. These typical features are the proof of abrasive wear [25,26]. AN et al [4] suggested that such features are the abrasive wear, in which hard asperities or particles cause wear by ploughing or cutting into the counterface alloys. Such features are present in all the tested conditions mixed with other wear mechanisms. Meanwhile, plenty of fine debris is found on the worn surface. As the load increases to 10 N, the grooves become deep and the plastic deformation is evident, as shown in Fig. 5(b). The surface is smooth and the amount of wear debris on the surface decreases significantly. Higher normal load would accelerate the surface and subsurface damage [9]. The wear mechanism tends to be an abrasion and plastic deformation at high normal load such as 10, 15 and 25 N for Mg−10Y−4Gd−1.5Zn−0.4Zr alloy.

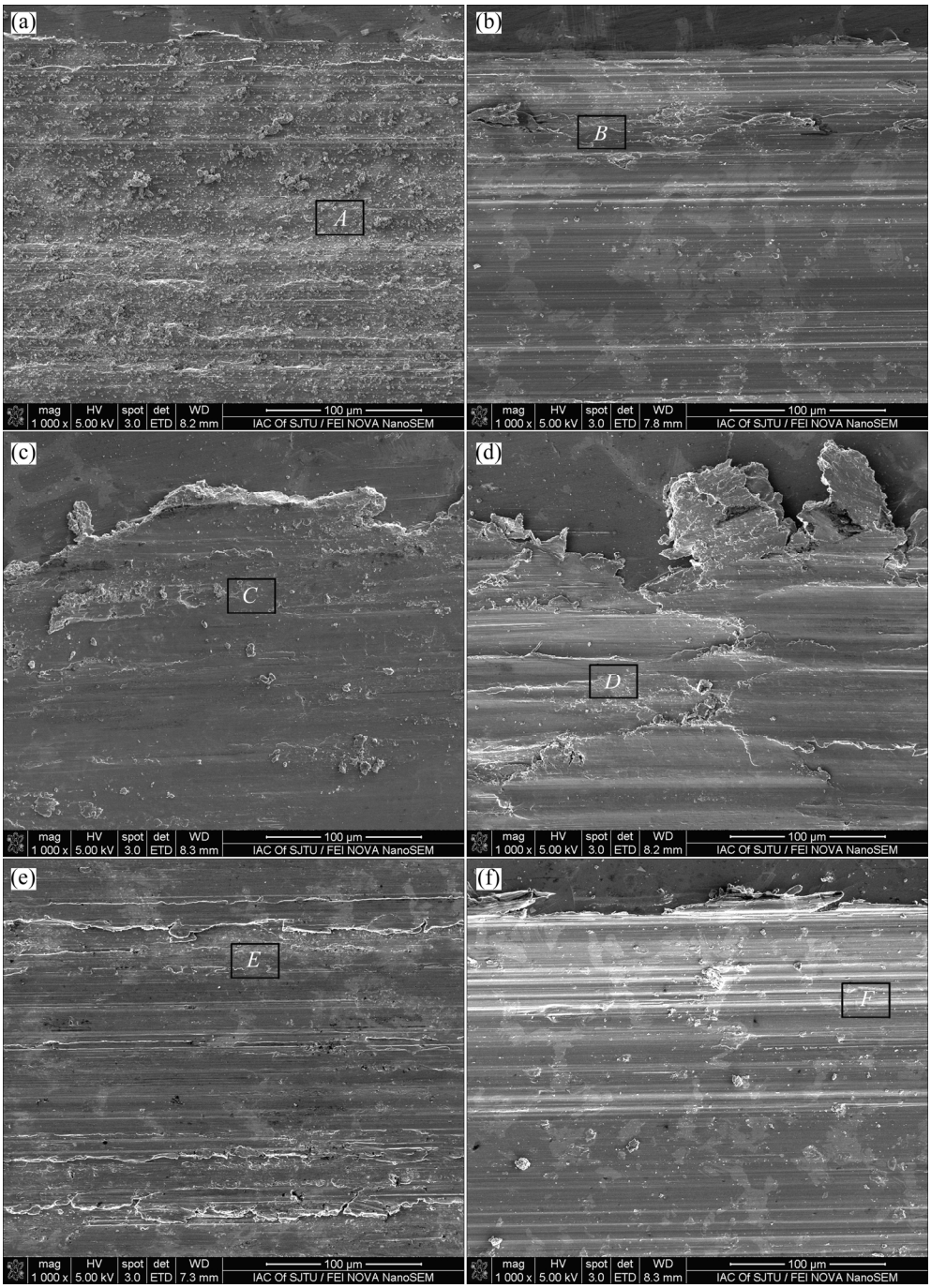

Fig. 5 SEM images of worn surfaces of cast+T6 Mg−10Y−4Gd−1.5Zn−0.4Zr alloy: (a) 0.06 m/s, 3 N, 25 °C, 400 m; (b) 0.06 m/s, 10 N, 25 °C, 400 m; (c) 0.18 m/s, 10 N, 25 °C, 400 m; (d) 0.3 m/s, 10 N, 25 °C, 400 m; (e) 0.06 m/s, 10 N, 100 °C, 400 m; (f) 0.06 m/s, 10 N, 200 °C, 400 m

As the speed increases to 0.18 m/s, the plastic deformation of the flat sample continues to increase, resulting in severely deformed layers. These layers were extruded from the interface, as shown in Fig. 5(c). These layers are 10−60 mm in length and 5−10 mm in thickness. These layers are spread out of the contact surface and easy to detach from the flat samples. It is interesting that these layers are observed on the contact surfaces at higher sliding speeds such as 0.12, 0.18, 0.24 and 0.3 m/s. Their length and thickness increase with increasing the sliding speed and the maximum layer is about 200 μm in length at the sliding speed of 0.3 m/s, as shown in Fig. 5(d). At high sliding speed, some wear debris is easy to be trapped in the wear system. The trapped debris is severely sheared and fragmented to fine particles in the subsequent sliding process. A part of fine particles and deformed alloy are compacted and extruded from the interface. At the same time, high relative motion generates more frictional heat, which improves the contact temperature. As the contact temperature increases, the alloy in the wear system is prone to plastic deformation. As a consequence, these layers near the contact surface form. On the other hand, the trapped debris was recycled in the wear system and reduced the wear rate, as shown in Fig. 3. Meanwhile, fine cracks can be found at the edge of smooth area. Most of the cracks are perpendicular to the sliding direction. In the previous studies, this typical feature was the proof of delamination [4,27]. It is noticeable from the EDS results that the content of O element increases with increasing the sliding speed, indicating that the oxides form on the worn surface, as shown in Table 3. As a result, the delamination and oxidative wear are also the wear mechanism at high sliding speed such as 0.12, 0.18, 0.24 and 0.3 m/s.

As the sliding temperature increases to 100 and 200 °C, as shown in Figs. 5(e) and (f), respectively, the worn surface morphologies are similar to those at 25 °C. Their worn surfaces are covered with numerous grooves, which is generally the proof of abrasive wear [25,26]. By examining the average oxygen fraction over the worn surface, as shown in Table 3, the fraction of oxidized surface increases with increasing the sliding speed and temperature. The average oxygen fraction of testing area reaches 34.89% at 200 °C. It is generally thought that the oxide film plays an important role in improving the wear properties at higher sliding temperatures. At the sliding temperature lower than 100 °C, the wear rate of Mg−10Y−4Gd−1.5Zn−0.4Zr alloy increases with increasing the sliding temperature, as expected in Ref. [9]. At the sliding temperature higher than 100 °C, the oxidation of the worn surface and trapped debris continues to increase, as shown in Table 3. The formed oxide film effectively protects the worn surface during the subsequent sliding wear. It is difficult to establish the severe abrasive between fresh Mg−10Y−4Gd−1.5Zn−0.4Zr alloy and the steel counterface, resulting in low wear rate. So, the wear rate decreases with increasing the sliding temperature from 100 to 200 °C, as shown in Fig. 4. As a result, it is interesting that a maximum value appears at 100 °C for Mg−10Y−4Gd−1.5Zn−0.4Zr alloy.

Table 3 EDS results of worn surfaces of cast+T6 Mg−10Y−4Gd−1.5Zn−0.4Zr alloy in Fig. 5 (mass fraction, %)

Testing area	Mg	Y	Gd	Zn	Zr	Fe	O	Total
A	79.02	9.16	5.16	1.62	0.14	0.08	4.82	100
B	80.3	10.06	4.98	1.56	0.34	0.10	2.66	100
C	74.12	9.92	4.69	1.47	0.31	0.26	9.23	100
D	63.35	7.73	3.01	0.99	0.12	0.32	24.48	100
E	68.56	5.24	4.02	0.85	0.10	0.08	21.15	100
F	53.89	5.46	4.15	1.36	0.13	0.12	34.89	100

3.4 Wear debris

The wear debris of cast+T6 Mg−10Y−4Gd−1.5Zn−0.4Zr alloy was carefully collected after each wear test. Figure 6 shows the SEM images of the wear debris of cast+T6 Mg−10Y−4Gd−1.5Zn−0.4Zr alloy. At low load of 3 N, the flat surface was subjected to mild ploughing and its wear debris is very fine, as shown in Fig. 6(a). The average size of these particles is usually 3−12 μm in length. These particles are easy to adhere to the worn surface, as shown in Fig. 5(a). It is beneficial for minimizing the worn surface damage and results in a relatively low wear mass loss, as shown in Fig. 2. As the load increases to 10 N, the wear debris increases in length and thickness, as shown in Fig. 6(b). The average size of these particles is usually 6−20 μm in length. The maximum size reaches up to 200 μm in length. This agrees well with the high wear rate.

As the sliding speed increases to 0.18 m/s, the wear debris continues to increase in length and thickness, as shown in Fig. 6(c). Some large blocky debris appears. It is noticeable that the large blocky debris reaches about 250 μm in length with increasing the sliding speed to 0.3 m/s, as shown in Fig. 6(d). The blocky debris is those layers formed near the contact surface, as shown in Figs. 5(c) and (d). This confirms that these layers are easy to detach from the contact surface of flat samples. On the other hand, the large blocky debris is easy to break into fragments.

As the sliding temperature increases to 100 and 200 °C, as shown in Figs. 6(e) and (f), the fine particles disappear and the morphology of debris changes to short plate-like particles. Meanwhile, the average size of these particles increases significantly in thickness. At higher sliding temperature, the wear debris and worn surface are

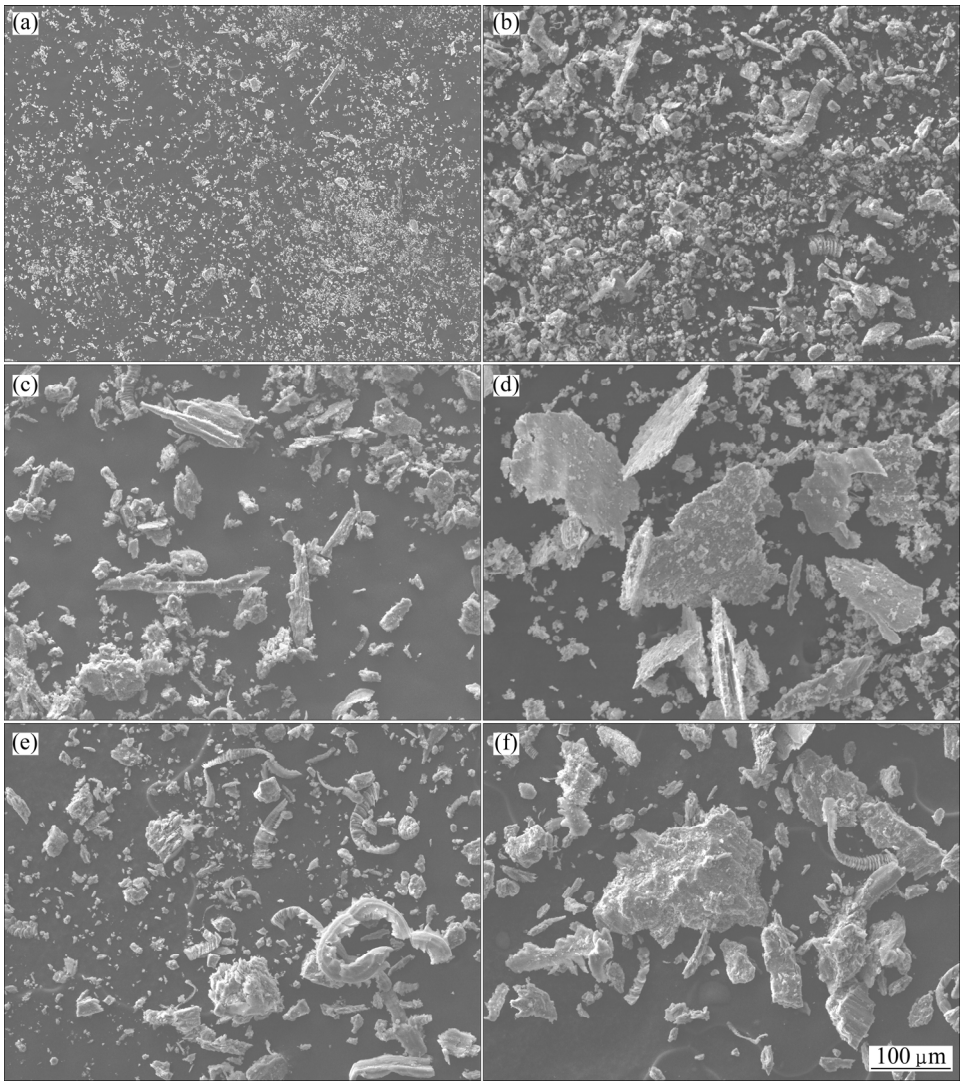

Fig. 6 SEM images of wear debris of cast+T6 Mg−10Y−4Gd−1.5Zn−0.4Zr alloy: (a) 0.06 m/s, 3 N, 25 °C, 400 m; (b) 0.06 m/s, 10 N, 25 °C, 400 m; (c) 0.18 m/s, 10 N, 25 °C, 400 m; (d) 0.3 m/s, 10 N, 25 °C, 400 m; (e) 0.06 m/s, 10 N, 100 °C, 400 m; (f) 0.06 m/s, 10 N, 200 °C, 400 m

easy to be oxidized. Meanwhile, the wear debris and worn surface get softened. It is easy to compact the material in the wear system to form the plate-like particles. These particles are easy to adhere to the steel counterface and protect the worn surface. The wear rate descends at higher sliding temperature from 100 to 200 °C.

4 Conclusions

1) The wear rates of as-cast and cast+T6 Mg−10Y−4Gd−1.5Zn−0.4Zr alloys are lower than that of cast+T6 AC9B aluminium alloy within a load range of 3−25 N, a sliding speed range of 0.03−0.3 m/s and a sliding temperature range of 25−200 °C at a constant sliding distance of 400 m.

2) For the Mg−10Y−4Gd−1.5Zn−0.4Zr alloy, the dominant mechanism is abrasion wear, which tends to be an abrasion and plastic deformation wear at high normal load such as 10−25 N, abrasion and plastic deformation wears with small participation of delamination and oxidative wears at high sliding speed such as 0.12−0.3 m/s, and an oxidative and abrasion wear at high test temperature such as 100−200 °C.

3) For the Mg−10Y−4Gd−1.5Zn−0.4Zr alloy, the effect of $Mg_{12}Y_1Zn_1$ phase on the wear resistance is higher than that of $Mg_{24}(GdYZn)_5$ phase at room temperature. At higher sliding speed (grater than 0.12 m/s) or higher sliding temperature (greater than 100 °C), the effect of $Mg_{12}Y_1Zn_1$ phase on the wear resistance decreases.

References

[1] QI Qing-ju. Evaluation of sliding wear behavior of graphite particle-containing magnesium alloy composites [J]. Transactions of

Nonferrous Metals Society of China, 2006, 16(5): 1135−1140.
[2] LIU Wen-cai, JIANG Long-kang, CAO Liang, MEI Jun, WU Guo-hua, ZHANG Song, XIAO Lü, WANG Shao-hua, DING Wen-jiang. Fatigue behavior and plane-strain fracture toughness of sand-cast Mg−10Gd−3Y−0.5Zr magnesium alloy [J]. Materials and Design, 2014, 59: 466−474.
[3] LI Qiang, WANG Qu-dong, WANG Ying-xin, ZENG Xiao-qin, DING Wen-jiang. Effect of Nd and Y addition on microstructure and mechanical properties of as-cast Mg−Zn−Zr alloy [J]. Journal of Alloys and Compounds, 2007, 427(1−2): 115−123.
[4] AN J, LI R G, LU Y, CHEN C M, XU Y, CHEN X, WANG L M. Dry sliding wear behavior of magnesium alloys [J]. Wear, 2008, 265(1−2): 97−104.
[5] DAS S, MORALES A T, ALPAS A T. Microstructural evolution during high temperature sliding wear of Mg−3%Al−1%Zn (AZ31) alloy [J]. Wear, 2010, 268(1−2): 94−103.
[6] FOUAD Y, EIBATANOUNY M. Effect of surface treatment on wear behavior of magnesium alloy AZ31 [J]. Alexandria Engineering Journal, 2011, 50(1): 19−22.
[7] SAENGSAI A, MIYASHITA Y, MUTOH Y. Effects of humidity and contact material on fretting fatigue behavior of an extruded AZ61 magnesium alloy [J]. Tribology International, 2009, 42: 1346−1351.
[8] EI-MORSY A W. Dry sliding wear behavior of hot deformed magnesium AZ61 alloy as influenced by the sliding conditions [J]. Materials Science and Engineering A, 2008, 473: 330−335.
[9] CHEN H, ALPAS A T. Sliding wear map for the magnesium alloy Mg−9Al−0.9Zn (AZ91) [J]. Wear, 2000, 246: 106−116.
[10] SHANTHI M, LIM C Y H, LU L. Effects of grain size on the wear of recycled AZ91 Mg [J]. Tribology International, 2007, 40: 335−338.
[11] DAVIDHANNA M. Tribological evaluation of aluminum and magnesium sheet forming at high temperatures [J]. Wear, 2009, 267: 1046−1050.
[12] MEHTA D S, MASOOD S H, SONG W Q. Investigation of wear properties of magnesium and aluminum alloys for automotive applications [J]. Journal of Materials Processing Technology, 2004, 155−156: 1526−1531.
[13] HU Mao-liang, WANG Qu-dong, CHEN Chang-jiang, YIN Dong-di, DING Wen-jiang, JI Ze-sheng. Dry sliding wear behaviour of Mg−10Gd−3Y−0.4Zr alloy [J]. Materials and Design, 2012, 42: 223−229.
[14] HU Mao-liang, WANG Qu-dong, LI Cheng, DING Wen-jiang. Dry sliding wear behavior of cast Mg−11Y−5Gd−2Zn magnesium alloy [J]. Transactions of Nonferrous Metals Society of China, 2012, 22(8): 1918−1923.
[15] ZEREN M. The effect of heat-treatment on aluminum-based piston alloys [J]. Materials and Design, 2007, 28(9): 2511−2517.
[16] XU C L, WANG H Y, LIU C, JIANG Q C. Growth of octahedral primary silicon in cast hypereutectic Al−Si alloys [J]. Journal of Crystal Growth, 2006, 291(2): 540−547.
[17] ASTM G133−02. Standard test method for linearly reciprocating ball-on-flat sliding wear [S].
[18] CHEN M, ALPAS A T. Ultra-mild wear of a hypereutectic Al−18.5wt.% Si alloy [J]. Wear, 2008, 265(1−2): 186−195.
[19] DWIVEDI D K. Wear behaviour of cast hypereutectic aluminium silicon alloys [J]. Materials and Design, 2006, 27(7): 610−616.
[20] ALSHMRI F, ATKINSON H V, HAINSWORTH S V, HAIDON C, LAWES S D A. Dry sliding wear of aluminium-high silicon hypereutectic alloys [J]. Wear, 2014, 313(1−2): 106−116.
[21] WANG Qu-dong, GAO Yan, YIN Dong-di, CHEN Chang-jiang. Characterization of phases in Mg−10Y−5Gd−2Zn−0.5Zr alloy processed by heat treatment [J]. Transactions of Nonferrous Metals Society of China, 2010, 20(11): 2076−2080.
[22] CHEN C J, WANG Q D, YIN D D. Thermal properties of Mg−11Y−5Gd−2Zn−0.5Zr (wt.%) alloy [J]. Journal of Alloys and Compounds, 2009, 487: 560−563.
[23] SUN Ming, WU Guo-hua, WANG Wei, DING Wen-jiang. Effect of Zr on the microstructure, mechanical properties and corrosion resistance of Mg−10Gd−3Y magnesium alloy [J]. Materials Science and Engineering A, 2009, 523: 145−151.
[24] MU Y L, WANG Q D, HU M L, JANIK V, YIN D D. Elevated-temperature impact toughness of Mg−(Gd, Y)−Zr alloy [J]. Scripta Materialia, 2013, 68: 885−888.
[25] AUNG N N, ZHOU W, LIM L E N. Wear behaviour of AZ91D alloy at low sliding speeds [J]. Wear, 2008, 265: 780−786.
[26] JIANG Jing, BI Guang-li, ZHAO Lei, LI Rong-guang, LIAN Jian-she, JIANG Zhong-hao. Dry sliding wear behavior of extruded Mg−Sn−Yb alloy [J]. Journal of Rare Earths, 2015, 33(1): 77−85.
[27] ZHANG J, ALPAS A T. Transition between mild and severe wear in aluminium alloys [J]. Acta Materialia, 1997, 45: 513−528.

Mg−10Y−4Gd−1.5Zn−0.4Zr 合金的摩擦磨损行为

胡茂良[1]，王渠东[2]，吉泽升[1]，许红雨[1]，辛明德[1]，马国睿[3]

1. 哈尔滨理工大学 材料科学与工程学院，哈尔滨 150040；
2. 上海交通大学 轻合金精密成型国家工程研究中心，上海 200240；
3. 哈尔滨工程大学 材料科学与化学工程学院，哈尔滨 150001

摘 要：采用球平面滑动摩擦试验机研究 Mg−10Y−4Gd−1.5Zn−0.4Zr 合金的摩擦磨损行为，对磨副选用 AISI 52100 型轴承钢球。研究在摩擦距离(400 m)不变的条件下，载荷(3~25 N)、摩擦速度(0.03~0.3 m/s)及摩擦温度(25~200 °C)对磨损率的影响。通过 SEM 和 EDS 分析合金试样的磨损表面和磨屑形貌，并在相同的摩擦磨损条件下，选用一种过共晶 Al−Si 合金进行对比性的摩擦磨损实验。结果表明：铸态和 T6 态 Mg−10Y−4Gd−1.5Zn−0.4Zr 合金的磨损率低于 T6 态过共晶 AC9B 铝合金的磨损率。T6 态 Mg−10Y−4Gd−1.5Zn−0.4Zr 合金的主要磨损机制是粘着磨损，高载荷(10~25 N)条件下趋于粘着磨损和塑性变形混合磨损机制；高摩擦速度(0.12~0.3 m/s)条件下趋于粘着磨损和塑性变形，并伴有剥层磨损和氧化磨损；高温(100~200 °C)条件下趋于氧化磨损和粘着磨损混合磨损机制。Mg−10Y−4Gd−1.5Zn−0.4Zr 合金中 $Mg_{12}Y_1Zn_1$ 相的数量及稳定性直接影响合金的磨损率。

关键词：Mg−Y−Gd−Zn−Zr 合金；滑动摩擦；磨损率；磨损机制；过共晶 Al−Si 合金

(Edited by Mu-lan QIN)